A cloned classical swine fever virus derived from the vaccine strain GPE$^-$ causes cytopathic effect in CPK-NS cells via type-I interferon-dependent necroptosis

Yukari Itakura [ORCiD: 0000-0002-3463-1834][1, †], Keita Matsuno [ORCiD: 0000-0002-4205-6526][1, 2, †], Asako Ito[1], Markus Gerber[3, 4], Matthias Liniger[3, 4], Yuri Fujimoto[1, a], Tomokazu Tamura [ORCiD: 0000-0003-1395-6610][1, b], Ken-ichiro Kameyama[1, c], Masatoshi Okamatsu [ORCiD: 0000-0002-0167-2285][1], Nicolas Ruggli [ORCiD: 0000-0002-7679-6290][3, 4], Hiroshi Kida[2, 5], Yoshihiro Sakoda [ORCiD: 0000-0001-7021-1688][1, 2*]

[†] These authors contributed equally to this work.

Author affiliations:

[1] Laboratory of Microbiology, Faculty of Veterinary Medicine, Hokkaido University, Sapporo 060-0818, Japan.

[2] Global Station for Zoonotic Control, Global Institution for Collaborative Research and Education (GI-CoRE), Hokkaido University, Sapporo, Hokkaido 001-0020, Japan.

[3] Institute of Virology and Immunology (IVI), Mittelhäusern and Bern, Switzerland.

[4] Department of Infectious Diseases and Pathobiology, University of Bern, Switzerland.

[5] Laboratory of Biologics Development, Research Center for Zoonosis Control, Hokkaido University, Sapporo, Hokkaido 001-0020, Japan.

[*]**Correspondence author**:

E-mail: sakoda@vetmed.hokudai.ac.jp

Postal address: Laboratory of Microbiology, Faculty of Veterinary Medicine, Hokkaido University, North 18, West 9, Kita-ku, Sapporo 060-0818, Hokkaido, JAPAN

Present address

[a] Veterinary Epidemiology Unit, Graduate School of Veterinary Medicine, Rakuno Gakuen University, Ebetsu, Hokkaido 069-8501, Japan.

[b] Department of Molecular Virology, Research Institute for Microbial Diseases, Osaka University, 3-1 Yamadaoka, Suita-shi, Osaka 565-0871, Japan.

[c] Exotic Disease Research Unit, Division of Transboundary Animal Disease, National Institute of Animal Health, NARO, Tsukuba, Ibaraki 305-0856, Japan.

Abstract

Classical swine fever viruses (CSFVs) do typically not show cytopathic effect (CPE) in cell culture, while some strains such as the GPE$^-$ vaccine induce CPE in the swine kidney-derived CPK-NS cell line cultured in serum-free medium. These latter strains commonly lack N^{pro}-mediated inhibition of type-I interferon (IFN) induction. In order to explore the molecular mechanisms of GPE$^-$-induced CPE, we analyzed the cellular pathways involved. In CPK-NS cells infected with the attenuated vGPE$^-$ strain, both, apoptosis and necroptosis were induced. Necroptosis was type-I IFN-dependent and critical for visible CPE. In contrast, the parental virulent vALD-A76 strain did not induce any of these pathways nor CPE. We used reverse genetics to investigate which viral factors regulate these cell-death pathways. Interestingly, a mutant vGPE$^-$ in which the N^{pro} function was restored to inhibit type-I IFN induction did not induce necroptosis nor CPE but still induced apoptosis, while an N^{pro}-mutant vALD-A76 incapable of inhibiting type-I IFN production induced necroptosis and CPE. Although E^{rns} of CSFV is reportedly involved in controlling apoptosis, apoptosis induction by vGPE$^-$ or apoptosis inhibition by vALD-A76 were independent of the unique amino acid difference found in E^{rns} of these two strains. Altogether, these results demonstrate that type-I IFN-dependent necroptosis related to non-functional N^{pro} is the main mechanism for CPE induction by vGPE$^-$, and that viral factor(s) other than E^{rns} may induce or inhibit apoptosis in vGPE$^-$ or vALD-A76 infected CPK-NS cells, respectively.

Keywords: classical swine fever virus, necroptosis, apoptosis, type-I interferon

1. Introduction

Classical swine fever virus (CSFV) is the causative agent of classical swine fever (CSF), a severe multisystemic disease that is a major threat to pig production. The clinical signs of CSF in pigs are highly diverse, ranging from subclinical infection to a hemorrhagic fever-like illness with high mortality [1]. Due to its global impact on the pig industry, CSF is notifiable to the World Organisation for Animal Health (OIE) [2, 3]. CSFV is an enveloped RNA virus, recently re-defined as a single member of the species *Pestivirus C* [4] within the *Pestivirus* genus of the *Flaviviridae* family along with the bovine viral diarrhea virus (BVDV) and border disease virus (BDV) [2, 5]. The CSFV virion carries a positive-sense single-stranded RNA genome possessing one large open reading frame (ORF), flanked by 5′ and 3′ untranslated regions (UTRs). The ORF encodes a single polyprotein cleaved co- and post-translationally by cellular and viral proteases into four structural proteins (C, E^{rns}, E1 and E2) and eight nonstructural proteins (N^{pro}, p7, NS2, NS3, NS4A, NS4B, NS5A and NS5B) [5]. Pestiviruses possess two unique proteins, N^{pro} and E^{rns}, which are missing in other *Flaviviridae* members. E^{rns} and N^{pro} have been associated with the regulation of type-I interferon (IFN) induction and cell-death during CSFV infection (for review, see [6]). The RNase activity of E^{rns} degrades single-stranded and double-stranded RNA to prevent type-I IFN induction and protein kinase R (PKR) activation [7, 8]. PKR is involved in apoptosis and programmed necrosis, also referred to as necroptosis [9]. N^{pro} is not essential for virus replication and degrades cellular interferon regulatory factor 3 (IRF-3), which prevents

type-I IFN production in non-plasmacytoid dendritic cells [6, 10−15]. The inhibition of type-I IFN production in swine testicle-derived cells infected with CSFV exalts a cytopathic effect (CPE) caused by superinfection with Newcastle disease virus. The exaltation of the Newcastle disease virus (END) phenomenon has been used to detect CSFV infection, which normally does not cause CPE in cultured cells [16].

Interestingly, several CSFV strains including field isolates lack the inhibitory activity of type-I IFN production [17, 18] and consequently do not show the END phenomenon [END-negative (END^-)]. These END^- strains induce clear CPE in CPK-NS and FS-L3 cells cultured under serum-free conditions [19, 20]. The combination of an END^- strain (*e.g.* Japanese live-attenuated vaccine strain GPE^-) and serum-free cultured cells has been used for CPE-based assays with CSFV such as neutralization tests [19, 20]. In contrast, END-positive (END^+) strains that inhibit type-I IFN production do not cause CPE in these and other cells, even under serum-free conditions. In addition to the inhibition of type-I IFN production, END^+ strains inhibit apoptosis induced by double-stranded RNA [21]. Thus, the cell-death observed as CPE in CPK-NS cells is likely to be associated with type-I IFN provoked by CSFV END^- infection and/or apoptosis regulation in these cells.

CPE following virus infection is considered to be the result of interaction between host defensive and viral anti-defensive activities leading to non-programmed necrosis, programmed apoptosis or other types of cell suicide, such as programmed necrosis (necroptosis) [22] and

inflammatory pyroptosis [23]. Necroptosis was recently reported as a caspase-independent cell-death initiated by tumor necrosis factor-α (TNF-α) with the same morphological features as necrosis [24], whereas apoptosis is well-known to be dependent on caspase activation [23]. In addition to TNF-α, necroptosis is induced by various stimuli such as the Fas ligand, the TNF-related apoptosis-inducing ligand, type-I IFN, pathogen-associated molecular patterns *via* Toll-like receptor activation, or DNA-dependent activator of IRFs activated by virus infection [25]. While apoptosis following viral infection has been extensively investigated, necroptosis in the context of virus infections has only been described thus far for influenza A virus [26], herpes simplex virus-1 and -2 [27, 28], murine cytomegalovirus [29], vaccinia virus [30], and reovirus [31].

In order to further understand CSFV-host cell interactions during CPE regulation, we investigated cell-death signaling pathways in CPK-NS cells infected with the cDNA-derived CSFV vGPE^{-} vaccine strain. We demonstrated that vGPE^{-} infection induced type-I IFN-dependent necroptosis, leading to CPE in CPK-NS cells. In addition, the apoptotic pathway was upregulated following vGPE^{-} infection, while the virulent vALD-A76 strain did not exhibit CPE nor stimulate necroptosis nor apoptosis. Importantly, CSFV N^{pro} was responsible for determining CPE while E^{rns} had no effect, although both were described to be involved in apoptosis regulation. These results provide new insights into CSFV-host cell interactions *in vitro*.

2. Materials and methods

2.1. Cells

The porcine kidney-derived CPK-NS cell line was established by culturing CPK cells in medium without serum. CPK-NS cells form unique fluid-filled multicellular domes on cell monolayers [19]. CPK-NS cells were grown in Eagle's Minimum Essential Medium (EMEM; Nissui Pharmaceutical) supplemented with $NaHCO_3$ and 1% anti-BVDV-antibody free fetal bovine serum (Japan Bio Serum). CPK cells were propagated in EMEM supplemented with 0.295% tryptose phosphate broth (TPB), 10 mM N, N-bis-(2-hydroxyethyl)-2-aminoethanesulfonic acid (BES), and 5% horse serum (Thermo Fisher Scientific). The porcine kidney SK-6 cells [32] were propagated in EMEM supplemented with 7% horse serum (SVA, Hatunaholm). The human embryonic kidney cell line 293T was maintained in Dulbecco's Modified Eagle's Medium (Thermo Fisher Scientific) supplemented with 10% fetal calf serum (Cambrex). All cells were incubated at 37°C in the presence of 5% CO_2.

2.2. Plasmids

The cDNA fragments of the ALD/A76 strain obtained by RT-PCR were cloned into the pACNR1180 vector by replacing the viral sequence of $pGPE^-$ [12, 33, 34]. The cDNA sequence was flanked by a modified T7 promoter sequence at the 5′end and a *Srf*I restriction site at the 3′end in analogy to a construct described previously [12]. Two mutant ALD/A76 cDNA clones

possessing either the amino acid substitution D136N in N^{pro} or N362S in E^{rns} of the pALD-A76 backbone were constructed by site-directed mutagenesis using KOD FX Neo (TOYOBO) and primers containing the mutation, and were named pALD-A76/D136N and pALD-A76/N362S, respectively. The full-length cDNA clone pEy/H297K with RNase inactive E^{rns} was obtained by site-directed mutagenesis of plasmid pEy-37 carrying a genome copy of the highly virulent Eystrup strain [35]. Briefly, a PCR fragment using pEy-37 as template was generated with overlapping primers encoding the H (cat) to K (aaa) mutation at amino acid position 297 of the CSFV Eystrup ORF (amino acid position 30 of E^{rns}) and used to replace the 1662 base pair ClaI to NgoMIV cassette in pEy-37. The complete sequences of the mutated cDNA plasmids were verified using Sanger sequencing.

2.3. Viruses

The following cDNA clone-derived CSFV were used in this study: a live-attenuated vaccine strain $vGPE^-$ [12, 33], a virulent strain vALD-A76, the mutants $vGPE^-$/N136D [12], vALD-A76/D136N and vALD-A76/N362S, and an RNase-deficient CSFV vEy/H297K. $vGPE^-$ and vALD-A76 are END^- and END^+ CSFV, respectively. The sequence used for the generation of $vGPE^-$ was derived from the original vaccine strain GPE^- after adaptation to swine kidney cell lines. The original virulent ALD-A76 strain is the parental strain of GPE^- strain.

For the rescue of infectious viruses, plasmids (*i.e.* $pGPE^-$, pALD-A76 and mutants, and

pEy/H297K) were linearized at the *Srf*I site located at the end of the viral genomic cDNA sequence and RNA was obtained by run-off transcription using the MEGAscript T7 kit (Thermo Fisher Scientific). After DNase I digestion and purification on S-400 HR Sephadex columns (GE Healthcare), RNA was transfected to SK-L cells by electroporation using Gene Pulser Xcell (Bio-Rad), and then incubated at 37°C for 3 days. Virus recovery was confirmed by immunostaining using an anti-CSFV NS3 antibody, and rescued clones were stored at −80°C.

For propagation, CSFV clones were inoculated to suspended SK-6 cells and incubated at 37°C for 3 days. Vesicular stomatitis virus (VSV), New Jersey strain, was also grown in SK-6 cells by inoculation to monolayered cells followed by incubation at 37°C overnight.

2.4. Sodium dodecyl sulfate-polyacrylamide gel electrophoresis (SDS-PAGE) and Western blot analysis

Cell monolayers were washed twice using PBS and lysed for 20 min on ice with a lysis buffer [0.1 M Tris-HCl (pH 7.6), 0.1 M NaCl, 1% Nonidat P-40 (Nacalai tesque), 1% Triton X-100 and cOmplete, Mini Protease Inhibition Cocktail, EDTA-Free tablet (Sigma-Aldrich)]. Lysates were then centrifuged at 14,500×g for 20 min at 4°C. The supernatants were mixed with SDS-PAGE sample-loading buffer [0.1 M Tris-HCl (pH 6.8), 4% SDS (Nacalai tesque), 10% 2-mercaptoethanol (Merck, Germany), 20% glycerol (FUJIFILM Wako Pure Chemical Corporation) and 0.005 % bromophenol blue (KISHIDA CHEMICAL)] and boiled for 5 min

followed by SDS-PAGE. The concentrations of the SDS polyacrylamide gels were 7.5% for NS3 and poly (ADP-ribose) polymerase (PARP), 10% for CSFV E2 and β-actin, 12% for caspase-3, glyceraldehyde 3-phosphate dehydrogenase (GAPDH), mixed lineage kinase domain like pseudokinase (MLKL), and phosphorylated MLKL, and 15% for swine IFN-α (swIFN-α). The separated proteins were transferred electrophoretically to an Immobilon-P PVDF Membrane (Merck) for immunodetection by chemiluminescence or to Immun-Blot LF PVDF membranes (Bio-Rad Laboratories) for immunodetection with IRDye-conjugated secondary antibodies (LI-COR). The membranes were treated with 5% non-fat milk or with Odyssey Blocking Reagent (LI-COR) and then incubated at 4°C overnight with primary antibodies against the following proteins: PARP (A2432; ABclonal), MLKL (A5579; ABclonal), Caspase-3 (A2156; ABclonal), phosphorylated MLKL (ab187091; Abcam), GAPDH (2118S; Cell Signaling Technology Japan), β-actin (C4, Santa Cruz Biotechnology), CSFV NS3 (46/1; [36]), or CSFV E2 (HC/TC26, [37]). Then, the membranes were washed for 10 min with PBST [0.05% Tween-20 (Nacalai tesque) in PBS] three times, and incubated with secondary antibodies at room temperature for 1 h. Goat anti-mouse IgG (H+L) horseradish peroxidase conjugate (Bio-Rad), goat anti-rabbit IgG (H+L) horseradish peroxidase conjugate (Bio-Rad) or goat anti-mouse IRDye680 (LI-COR) were used as the secondary antibodies. After three times of 10-min washing with PBST, the membranes were treated with Immobilon Western Detection Reagents (Merck) for chemiluminescence, or acquired directly with the Odyssey Infrared Imaging System (LI-COR) for near-infrared imaging.

For chemiluminescence, the protein signals were detected by WSE-6100H LuminoGraph I (ATTO) and analyzed by CS Analyzer 4 (ATTO).

2.5. Dot blotting

Two microliters of cell lysates obtained as described in section 2.4 were applied on an Immobilon-P PVDF Membrane and blocked in 5% non-fat milk for 1 h at room temperature. The membranes were then incubated with primary antibody for E2 (A301; [38]), which recognizes a conformational epitope of E2, for 1 h at room temperature, washed for 10 min with PBST three times and incubated with the secondary antibody; goat anti-mouse IgG (H+L) horseradish peroxidase conjugate at room temperature for 1 h. After three times of 10-min washing with PBST, membranes were treated with Immobilon Western Detection Reagents. Protein signals were detected using WSE-6100H LuminoGraph I and analyzed with CS Analyzer 4.

2.6. Recombinant swIFN-α

The cDNA fragment of swIFN-α fused with a 6x-histidine tag was obtained from the transcripts of CPK cells by RT-PCR and cloned into pCAGGS.MCS (pCAGGS/swIFN-α) [39, 40]. Recombinant swIFN-α was obtained as follows: 15 μg of pCAGGS/swIFN-α was

transfected into 293T cells cultured in a 100 mm dish after a 20-min incubation at room temperature with 1.5 ml of Opti-MEM I Reduced-Serum Medium and 45 μl of Trans-IT 293 Reagent (Takara Bio). After 48 h incubation at 37°C, the supernatant was collected, and swIFN-α was purified using AKTA prime plus and HisTrap^{TM} FF crude (GE Healthcare) according to the manufacturer's protocols with 400 mM imidazole for elution. The expression and bioactivity of swIFN-α were confirmed by using Western blotting and the VSV plaque inhibition test, respectively.

2.7. Titration of type-I IFN by VSV plaque inhibition

The VSV plaque inhibition test was performed as previously described [41]. Infectious CSFVs in the supernatant of virus-infected cells were inactivated by UV exposure (254 nm) using the UV Crosslinker (ATTO) for 20 min. To quantify the bioactivity of type-I IFN, samples were diluted at two-fold, and 1 ml of each diluted sample was added to SK-L cells cultured in 12-well plates followed by 24 h incubation at 37°C. Then, samples were removed and VSV was inoculated at 50 plaque forming units (PFU) per well for 1 h followed by overlaying 1 ml of TPB-MEM containing 0.7% Bacto Agar with 0.1% $NaHCO_3$ per well. After a 2-day incubation at 37°C, the TPB-MEM-agar mixture with 0.1% $NaHCO_3$ and 0.005% Neutral Red were overlaid. After 24 h of incubation, the type-I IFN titer was calculated as the reciprocal number of the highest dilution, which is equal to or less than 50% PFU of the negative control.

2.8. Antiserum against swIFN-α

Polyclonal antiserum against swIFN-α was prepared from mice immunized with recombinant swIFN-α. Fifty micrograms of recombinant swIFN-α mixed with the same amount of Adjuvant Incomplete Freund (Becton, Dickinson and Company) per mouse was inoculated subcutaneously twice with a two-week interval. Serum was obtained from each immunized mouse two weeks after the second immunization and used for neutralization tests. Neutralizing titer of the antiserum against swIFN-α was determined as the reciprocal number of the highest dilution, in which CPK-NS cells did not show CPE when treated with 2×10^5 unit/cell of swIFN-α.

2.9.Virus inoculation

CSFVs were inoculated onto confluent cell monolayers at the multiplicity of infection (MOI) of 1.0 $TCID_{50}$/cell. Cells were absorbed with CSFVs at 37°C for 1 h, followed by PBS wash and incubation with fresh medium with or without the following inhibitor at 37°C for the indicated time intervals: caspase-3 inhibitor Z-DEVD-FMK (50 μM; 4800-510), caspase-8 inhibitor Z-IETD-FMK (50 μM; 4805-510) (Medical & Biological Laboratory), or receptor interacting protein kinase-1 (RIPK1) inhibitor Necrostatin-1 (50 μM; N9037-10MG) (Sigma-Aldrich).

2.10. Cell viability

Cell viability was evaluated with Cell Counting Kit-8 (CCK-8) assay (DOJINDO LABORATORIES) according to the manufacturer's instructions. Briefly, 10 µl of CCK-8 solution was added to cells cultured in 96-well plates followed by incubation for 4 h at 37°C. The optical density was measured at 450 nm using MULTISCAN JX (Thermo Fisher Scientific). OD_{450} measurements in mock-infected cells were considered to be 100% viability.

2.11. Caspase-3/7 activity

Caspase-3/7 activity was quantified by using the Caspase-Glo-3/7 assay system (Promega) according to the manufacturer's instructions. Briefly, 30 µl of Caspase-3/7-Glo assay reagent was added to cells cultured in 96-well plates followed by incubation for 2 h at room temperature. The luminescence was measured using POWER SCAN 4 (BioTek).

2.12. RNase activity assay

A 50-mer RNA oligonucleotide probe complementary to nucleotides 12242-12193 of the vA187-1 genome sequence (GenBank accession number X87939.1) carrying a Dyomics 781 modification at the 5'-end (Dy-781-O1-RNA) was synthesized by Dr. Fabian Axthelm (Microsynth AG, Balgach, Switzerland). The Dy-781-O1-RNA probe was mixed at 40 nM final

concentration with MEM containing 3×10^{-3} U RNase A/ml as digestion control and with the samples to be tested for RNase activity and incubated for 1 h at 37°C. The treated probes were then mixed with 2 volumes of 97% Formamide (Sigma) and separated on a 10% polyacrylamide and 35% urea gel in 133 mM TrisHCl, 45.5 mM boric acid and 3.2 mM EDTA. Image acquisition was performed with the Odyssey Infrared Imaging System (LI-COR).

2.13. Statistical analysis

Statistically significant differences were defined using the Student's *t*-test.

3. Results

3.1. CSFV vGPE$^-$ infection induces type-I IFN production and CPE in CPK-NS cells.

There are four amino acid differences in N^{pro} between vGPE$^-$ and the parent vALD-A76 (residues 5, 27, 32 and 136). N^{pro} is a metalloprotein and the aspartic acid at position 136 within the zinc-binding domain of N^{pro} of END$^+$ CSFV (Fig.1A) is critical for N^{pro} to mediate degradation of IRF-3 [12, 13, 14]. Accordingly, we swapped the amino acid residue 136 between vGPE$^-$ and vALD-A76 to generate a vGPE$^-$ mutant with functional N^{pro} in terms of IRF3 degradation (vGPE$^-$/N136D) and a vALD-A76 mutant with non-functional N^{pro} incapable of IRF3 degradation (vALD-A76/D136N). We then examined type-I IFN production and CPE in CPK-NS cells infected with these different viruses (Table 1). Using the VSV plaque inhibition

test, bioactive type-I IFN was detected at 72 and 96 hours post-infection (hpi) with vGPE$^-$ or vALD-A76/D136N, but not with vALD-A76 nor with vGPE$^-$/N136D. Consistent with our previous study [12], these results confirmed that inhibition of type-I IFN induction was dependent on aspartic acid 136 of CSFV N^{pro}. Under the microscopic evaluation, CPE started to appear from 72 hpi to 96 hpi in CPK-NS cells infected with vGPE$^-$ or vALD-A76/D136N and in cells treated with swIFN-α or the apoptosis inducer cisplatin (Fig. 1B). CPE induced by vGPE$^-$ in CPK-NS cells manifested as cell rounding and detachment, similar to CPE observed in swIFN-α- or cisplatin-treated cells. CPE was not observed in cells infected with vALD-A76 nor with vGPE$^-$/N136D (Table 1, Fig. 1B). Cells infected with vGPE$^-$ or vALD-A76/D136N, or treated with swIFN-α or cisplatin showed a significant decrease in cell viability, which was followed by clearly visible CPE. Interestingly, decreased viability was observed also with vGPE$^-$/N136D-infected cells (END$^+$) and began at 48 hpi similarly to vGPE$^-$, preceding the CPE observed with vGPE$^-$ at 72 hpi, while no CPE was observed with vGPE$^-$/N136D at any time (Fig. 1B, 1C). Of note, visible CPE was the result of less than 60% cell viability. In contrast to CPK-NS cells, the parental CPK cells [20] did not show any morphological changes when infected with vGPE$^-$ nor when treated with swIFN-α, even with significantly decreased cell viability (Fig. 1B, 1C). We examined also cell viability and CPE in five porcine cell lines exposed to different amounts of swIFN-α (Fig. S1). CPK-NS cells and SK-6 cells [42] showed notably decreased cell viability (Fig. S1) and obvious CPE (data not shown) with ≥10 unit/ml of swIFN-α in contrast to the other

cell lines tested, *i.e.* SK-L [43], FS-L3 [43], and CPK cells (Fig. S1). Despite the similar loss of viability of SK-6 and CPK-NS cells to swIFN-α treatment, SK-6 cells did not show any CPE nor cell-death in response to vGPE^{-} infection (data not shown), which may be related to the SK-6 deficiency in type-I IFN production [44]. These results indicated that cells with intact type-I IFN production and cell-death signaling pathways triggered by type-I IFN undergo CPE after vGPE^{-} infection. Importantly, vGPE^{-} infection or swIFN-α treatment in the presence of neutralizing antibodies against swIFN-α reduced CPE (Fig. 1D). Anti-swIFN-α antibodies also rescued the drop of cell viability after vGPE^{-} infection while the addition of anti-swIFN-α antibodies itself increased cell viability in CPK-NS cells (Fig. 1D, 1E). Taken together, the type-I IFN activity in CPK-NS cells infected with an END^{-} CSFV strain plays a critical role in CPE induction. However, cell-death starts before type-I IFN secretion and the appearance of CPE and is also observed with mutant vGPE^{-} in which the IFN inhibitory function of N^{pro} was restored (in absence of visible CPE), which suggests concomitant actions of different mechanisms and pathways leading to CPE and/or reduced cell viability following CSFV infection in CPK-NS cells.

3.2. vGPE^{-} infection elicits both, apoptosis and IFN-dependent necroptosis in CPK-NS cells.

Driven by the observations described above, different cell-death pathways induced by

vGPE⁻ were analyzed in CPK-NS cells. The viability of CPK-NS cells infected with vGPE⁻ in the presence of specific inhibitors of apoptosis or necroptosis was determined by using the CCK-8 assay (Fig. 2). Cell-death of CPK-NS cells caused by vGPE⁻ infection was prevented in the presence of the caspase-3 inhibitor, caspase-8 inhibitor, or RIPK1 inhibitor. Caspase-3 and caspase-8 inhibitors also abolished effector caspase activation in cisplatin-treated cells, but failed to block cell-death in cells treated with swIFN-α. In contrast, swIFN-α-treated cells were protected from death in the presence of the RIPK1 inhibitor. These results suggested that cell-death (not equivalent to CPE) induced by vGPE⁻ infection occurred via both, the apoptotic and necroptotic pathways. Type-I IFN treatment of CPK-NS cells triggered the necroptotic, but not the apoptotic, pathway.

3.3. The D136N substitution of N^{pro} is responsible for triggering CPE via IFN-dependent necroptosis, while other vGPE⁻ factors different from E^{rns} induce apoptosis.

In order to determine which cell-death pathways are activated in CPK-NS cells, the expression levels of cell-death-related proteins were assessed in CPK-NS cells under different infections or treatments (Fig. 3A, 3B and S2A). In cells infected with vGPE⁻, apoptosis-specific cleaved-caspase-3 was detected at 24 to 72 hpi followed by the detection of cleaved PARP until 96 hpi. The caspase-3 cleavage signals were weak which might be due to weak reactivity of the antibody for the cleaved form of caspase-3. This result indicated that the apoptotic pathway was

activated within 24 h following vGPE$^-$ infection and remained activated until 72 hpi; additionally, a significant proportion of cells underwent cell-death in the absence of visible CPE from 24 to 48 hpi (Fig. 1C). The expression levels of MLKL and phosphorylated MLKL, which are hallmarks of the activation of the necroptotic signaling cascade, were also significantly increased in vGPE$^-$-infected cells at 96 hpi, simultaneous to bioactive type-I IFN secretion (Fig. 3A, 3B, S2A and Table 1). In CPK cells, vGPE$^-$ infection did not cause any apparent increased expression of cell-death related proteins (Fig. 3A, S2B). Increased signals of MLKL and phosphorylated MLKL were also detected in swIFN-α-treated-CPK-NS cells. In vALD-A76-infected cells, there was no noticeable increase in any of the cell-death markers analyzed. Interestingly, vGPE$^-$/N136D (END$^+$) and vALD-A76/D136N (END$^-$) activated apoptosis and necroptosis, respectively (Fig. 3A, S2A). Caspase-3 and caspase-8 mRNA expression were increased in both, the vGPE$^-$- or vGPE$^-$/N136D-infected CPK-NS cells at 24 or 48 hpi as opposed to the vALD-A76- or vALD-A76/D136N-infected cells at 24 or 48 hpi (Fig. S3). mRNA expression of necroptosis-related factors RIPK1 and MLKL increased in the presence of type-I IFN in vGPE$^-$- or vALD-A76/D136N-infected cells at 72 and 96 hpi as well as swIFN-α-treated CPK-NS cells (Fig. S3). In contrast, there was only a slight increase in the mRNA expression of cell-death signaling factors detected in vGPE$^-$ infection and swIFN-α treatment in CPK cells (Fig. S4). Note that we observed an unexpected increase (not matched to protein expressions) of mRNA of caspase-3 or caspase-8 in swIFN-α treated cells or vALD-A76/D136N-infected cells,

respectively. These results show the induction of two distinct cell-death mechanisms by vGPE$^-$ infection in CPK-NS cells: IFN-independent apoptosis and IFN-dependent necroptosis. Furthermore, the activation of cell-death pathways in CPK-NS cells is differentially regulated compared to the pathways in parental CPK cells.

Caspase-3/7 activity was then assessed to reveal the activation of apoptotic factors in CPK-NS cells infected with different CSFVs. In cells infected with vGPE$^-$ or vGPE$^-$/N136D, the caspase activity was significantly higher than in cells infected with vALD-A76 or vALD-A76/D136N after 48 hpi (Fig. 4A). Active caspase-3/7 was detected mainly from 48 to 96 hpi, while the increased expression of cleaved-caspase-3 was detected at 24 and 48 hpi (Fig. 3A). Moreover, at 96 hpi, increased caspase-3/7 activity in vALD-A76/D136N-infected cells and decreased caspase-3/7 activity in vGPE$^-$/N136D-infected cells suggested that IFN signaling may slightly contribute to promoting caspase-3/7 activity, yet not detected as cleaved-caspase-3 expression. Next, to clarify the dose-dependency of apoptosis and necroptosis in CPK-NS cells infected with vGPE$^-$, CPK-NS cells were infected with serially diluted vGPE$^-$. Caspase-3/7 activity was not observed in cells infected with a lower titer (i.e. MOI = 0.1 or less) of vGPE$^-$ (Fig. 4B), while delayed but significant cell death was detected (Fig. 4C) with visible CPE (data not shown). Taken together, apoptosis is upregulated in CPK-NS cells infected with vGPE$^-$ but negligibly contributes to visible CPE as consequence of IFN-dependent necroptosis.

E^{rns} was reported to contribute to the inhibition of apoptosis in CSFV-infected cells [44].

There is a single amino acid difference at position 362 in E^{rns} of vGPE^{-} *versus* vALD-A76 (Fig. 5A). In order to evaluate whether this difference affects apoptosis in CPK-NS cells, caspase-3/7 activity and cell viability were compared in cells infected with vALD-A76 or vALD-A76/N362S (Fig. 5B, 5C). Infection with vALD-A76/N362S did not show any significant differences in caspase-3/7 activity nor in cell viability compared to vALD-A76 infection. (Fig. 5B, 5C). Additionally, RNase activity of E^{rns}, which plays a role in apoptosis regulation during CSFV infection, was evaluated for these two clones. The vALD-A76/N362S mutant showed the same specific RNase activity as the parent vALD-A76 (Fig. 5D). Expression of viral protein was confirmed by immunoblotting of E2 (Fig. 5E). These results show that the single amino acid difference in E^{rns} of vGPE^{-} compared with vALD-A76 is not responsible for whether CSFV induces apoptosis or not in CPK-NS cells. Therefore, besides the N^{pro}-dependent control of the necroptosis pathway, there may be other viral factor(s) different from E^{rns} by which vGPE^{-} activates or vALD-A76 inhibits the apoptosis signaling pathway.

3.4. NS2-3 cleavage and NS3 accumulation in CSFV-infected cells

In BVDV-infected cells, expression of cleaved-NS3 together with uncleaved-NS2-3 is recognized as a specific marker for cytopathogenic (cp) virus, whereas NS2-3 becomes substantial in cells infected with noncytopathogenic (ncp) BVDVs [5]. In order to address CSFV NS2-3 cleavage in CPK-NS cells infected with CSFV END^{-} strains displaying CPE, NS2-3 and

NS3 expression patterns were analyzed. For all CSFVs, NS2-3 and NS3 expression increased in a time-dependent manner (Fig. 6A). In vGPE^{-}- or vALD-A76/D136N-infected cells, the ratio between NS2-3 and NS3 greatly inclined towards NS3 when these viruses caused CPE in infected cells (Fig. 6B). In comparison with vGPE^{-}- or vALD-A76/D136N-infected cells, NS2-3 expression was higher in vGPE^{-}/N136D- or vALD-A76-infected cells (Fig. 6A). Interestingly, the expression of the viral protein E2 was also higher in vGPE^{-}/N136D- or vALD-A76-infected cells than in cells infected with vGPE^{-} or vALD-A76/D136N (Fig. 6C, 6D). Note that when CPE was induced by swIFN-α or cisplatin in CPK-NS cells infected with vALD-A76, the proportion of NS3 to NS2-3 increased, even though there was no actual increase in NS3 expression (Fig. 6E, 6F). These results suggest that the accumulation of CSFV NS3 is likely to be the result of interferon induction that might suppress virus protein synthesis.

4. Discussion

Nonspecific antiviral mechanisms, such as IFN-stimulated antiviral responses and IFN-dependent/independent cell-death, are targets of viral proteins to efficiently produce virions. Regarding CSFV, N^{pro} and E^{rns} are known to inhibit type-I IFN production and apoptosis induction [5]. To further understand host responses during CSFV infection, CPE following the infection of serum-free CPK-NS cells with the cloned vaccine strain vGPE^{-} was characterized in comparison with its parental strain vALD-A76, as a model of END^{-} and END^{+} CSFVs,

respectively. The present study demonstrated the induction of IFN-independent apoptosis followed by IFN-dependent necroptosis in vGPE$^-$-infected CPK-NS cells. The mechanism responsible for CPE in CPK-NS cells subsequent to vGPE$^-$ infection is likely to be IFN-dependent necroptosis, because the cells showed CPE via infection with a low titer of vGPE$^-$ that did not activate the apoptotic signaling pathway. Additionally, we demonstrated that the cloned virulent strain vALD-A76 inhibited the apoptotic pathway and IFN production as well as the necroptotic pathway (Fig. 7). Additional experiments with other pairs of END$^-$ and END$^+$ strains would be helpful for confirming the results obtained here with vGPE$^-$ and vALD-A76.

The present study reveals that the lack of N^{pro}-regulated inhibition of type I IFN-production is a key factor for CPE induction in CPK-NS cells. N^{pro} is a metalloprotein and several amino acid residues including D136 were identified as important elements in the zinc-binding site to interact with IRF-3 [13]. The inhibition of type-I IFN production and cell-death in vALD-A76-infected cells were clearly demonstrated *in vitro*, consistent with the previous study [46]. The participation of IFN signaling in necroptosis, as reported in reovirus infection [31], provides another explanation for the benefit of CSFV to inhibit type-I IFN production by means of N^{pro}, *i.e.* the escape from necroptosis in addition to the prevention an IFN-stimulated antiviral state in host cells. While vALD-A76 inhibits IFN production and consequently also necroptosis, high levels of IFN-α are detected in the serum of CSFV infected pigs, particularly with high virulent strains with functional N^{pro} [47]. This has been attributed to enhanced virus replication as a result

of N^{pro}-mediated suppression of local type-I IFN induction in the early stage of infection leading to elevated systemic type-I IFN responses by activated plasmacytoid dendritic cells [12]. Furthermore, the regulation of IFN-stimulated genes involved in apoptosis correlated with the severity of lymphopenia in CSFV infection in pigs [47], due to the indirect induction of apoptosis in non-infected neighboring cells, known as "bystander apoptosis" [48, 49]. As another mechanism to cause lymphopenia in CSFV infection, a recent study demonstrated that pyroptosis, an inflammatory caspase-dependent programmed cell-death, is associated with lymphocyte depletion and immunosuppression in CSFV-infected pigs [50].

The CSFV envelope protein E^{rns} was reported to regulate apoptosis induction. Amino acid substitutions to inactivate the RNase activity of E^{rns} modulates the ncp/cp phenotype of CSFV, even in non-serum-free porcine cell lines [45]. This can be explained by the lack of down-regulation of cellular RNAs, disrupting homeostasis in cells infected with RNase-deficient CSFVs and strongly inducing programmed cell-death. In addition, RNase activity can prevent cell-death signaling pathways mediated by double-stranded RNA [21]. Between $vGPE^{-}$ and vALD-A76, there is a single amino acid difference outside of the catalytic RNase domains of E^{rns}, and this amino acid was found here not to affect apoptosis induction. Thus, the E^{rns} of $vGPE^{-}$ and vALD-A76 is not responsible for determining whether infection induces or inhibits apoptosis in CPK-NS cells. These results suggest that other viral proteins suppress the apoptotic signaling pathway in CPK-NS cells infected with vALD-A76 or activate apoptosis in $vGPE^{-}$-infected cells.

Even though apoptosis is not primarily responsible for CPE induction and the mechanism is not clear yet, the apoptotic signaling pathway is activated in CPK-NS cells infected with vGPE$^-$ at early stages of infection (Supplemental Fig. S5) in accordance with our previous study detecting DNA fragmentation, a key marker of apoptosis, in CPK-NS cells infected with GPE$^-$ [20]. These results suggest the presence of E^{rns}-independent apoptosis regulation in CSFV infection.

In addition to the modulation of apoptosis induction by E^{rns} as reported previously, CSFV may escape from apoptosis by inducing mitophagy or autophagy to inhibit mitochondrial-dependent apoptosis or reactive oxygen species-dependent apoptosis enhancing persistent infection [51, 52]. The present study indicated that type-I IFN production and type-I IFN-dependent activation of the necroptotic pathway are required to induce CPE. Even though serum-free cultured FS-L3 cells did not show a drastic decrease in cell viability by swIFN-α, an approximately 20% decrease in cell viability was sufficient to lead to the disappearance of the unique fluid-filled multicellular domes on cell monolayers. The disappearance of domes was described previously to be caused by END$^-$ CSFV infection, but not by END$^+$ CSFV infection [19] as a result of the negative impact of IFN exposure. For future studies, the adaptation processes of the GPE$^-$ strain in guinea pig cells and CPK-NS cells and/or FS-L3 cells to serum-free medium should be investigated to unravel the rationale of selecting these biotypes.

NS3 expression is usually recognized as a specific marker for cp viruses in BVDV. NS2-3 of cp BVDV strains often contain insertions of cellular or viral sequences that enhance protein

processing of NS2-3 to NS3 [53]. For example, a cell-derived insertion of the J-domain protein interacting with viral protein (Jiv) gene promotes NS2-3 cleavage and cytopathogenicity of some cp BVDVs [53]. Although CSFV expresses NS3 regardless of the cp or ncp phenotype, contribution of cellular Jiv has not been addressed here. Field cp isolates of CSFV are believed to contain defective interfering (DI) particles that may alter the expression of NS3 [54], resulting in higher NS3 expression than ncp CSFVs that are able to express NS3 [38]. While BVDV NS2-3 of ncp viruses can block apoptosis in cells [53], the contribution(s) of the enhanced processing of NS2-3 into NS3 in the cytopathogenicity of pestiviruses has not been fully clarified. NS3 is a multifunctional enzyme and possesses serine protease, nucleoside triphosphatase, and RNA helicase activities [5]. In the present study, vGPE$^-$ infection-mediated apoptosis in CPK-NS cells and increased NS3:NS2-3 ratio was observed in CPE-exhibiting cells. However, there is no relationship between CPE and NS3 expression in this case. This may be due to the accumulation of NS3 prior to cell-death induction, the reduction of newly synthesized NS2-3, and/or upregulation(s) of cellular factors, such as Jiv. Hence, the relationship of NS2-3 cleavage and cytopathogenicity may vary among pestiviruses.

5. Conclusion

In summary, the present study demonstrated the mechanism of CPE and associated cell-death in porcine kidney-derived serum-free CPK-NS cells infected with END$^-$ CSFV and the

contributions of N^{pro} but not E^{rns} in cell-death regulation. Due to the importance of END^{-} CSFV-induced CPE in CPK-NS cells in the diagnosis in Japan, understanding the mechanism will facilitate the surety of diagnostic tests. Future studies may address the molecular mechanism(s) and the contribution of cell-death induced by CSFV infection not only with respect to cytopathogenicity *in vitro* but also to pathogenicity in pigs.

AUTHOR STATEMENTS

Conflicts of interest

The authors declare that there are no conflicts of interest.

Funding information

This study was partially funded by Grant-in-Aid for Scientific Research (B) (JSPS KAKENHI Grant Number: 19380170); Grant-in-Aid for Scientific Research on Innovative Areas from the Ministry of Education, Culture, Science, Sports, and Technology (MEXT) of Japan (MEXT KAKENHI Grant Numbers: JP19H03115, JP16H06429, JP16K21723, and JP16H06431); and the Japan Initiative for Global Research Network on Infectious Diseases (J-GRID) (Grant Number: PJ18fm0108008) from the Japan Agency for Medical Research and Development (AMED).

Ethics statement

The animal experiments were approved by the Institutional Animal Care and Use Committee of the Faculty of Veterinary Medicine, Hokkaido University (approval number 18-0035) and performed according to the committee's guidelines.

Acknowledgments

Our great appreciation is extended to M. Endo for the construction of pALD-A76 and Prof. Dr. O. Inanamai, Laboratory of Radiation Biology, Faculty of Veterinary Medicine, Hokkaido University, and Dr. H. Sawa, Division of Molecular Pathobiology, Research Center for Zoonosis Control, Hokkaido University for the discussion and critical review of the manuscript.

REFERENCES

1. **van Oirschot JT.** Classical Swine Fever (Hog Cholera). Disease of Swine, 8th ed., eds Brabara E, Straw BE, D'Allaire S, Mengeling WL, Taylor DJ (Wiley-Blackwell, Hoboken) 1999;1:159-172.
2. **Blome S, Beer M, Wernike K.** New Leaves in the Growing Tree of Pestiviruses. *Adv Virus Res* 2017;99:139–160.
3. **Moennig V, Becher P.** Pestivirus control programs: How far have we come and where are we going? *Anim Heal Res Rev* 2015;16:83–87.
4. **Smith DB, Meyers G, Bukh J, Gould EA, Monath T, Muerhoff AS, *et al.*** Proposed revision to the taxonomy of the genus *Pestivirus*, family *Flaviviridae*. *J Gen Virol* 2017;98:2106–2112.
5. **Tautz N, Tews BA, Meyers G.** The Molecular Biology of Pestiviruses. *Adv Virus Res* 2015;93:47–160.
6. **Summerfield A, Ruggli N.** Immune Responses Against Classical Swine Fever Virus: Between Ignorance and Lunacy. *Front Vet Sci* 2015;2:1–9.
7. **Lussi C, Sauter KS, Schweizer M.** Homodimerisation-independent cleavage of dsRNA by a pestiviral nicking endoribonuclease. *Sci Rep* 2018;8:1–11.
8. **Python S, Gerber M, Suter R, Ruggli N, Summerfield A.** Efficient Sensing of Infected Cells in Absence of Virus Particles by Blasmacytoid Dendritic Cells Is Blocked by the Viral Ribonuclease E^{rns}. *PLoS Pathog* 2013;9:e1003412.
9. **Sridharan H, Upton JW.** Programmed necrosis in microbial pathogenesis. *Trends Microbiol* 2014;22:199–207.
10. **Bauhofer O, Summerfield A, Sakoda Y, Tratschin J-D, Hofmann MA, Ruggli N.** Classical Swine Fever Virus N^{pro} Interacts with Interferon Regulatory Factor 3 and Induces Its Proteasomal Degradation. *J Virol* 2007;81:3087–3096.
11. **Rocca S La, Herbert R, Crooke H.** Loss of Interferon Regulatory Factor 3 in Cells Infected with Classical Swine Fever Virus Involves the N-Terminal Protease, N^{pro}. *J Virol* 2005;79:7239–7247.
12. **Tamura T, Nagashima N, Ruggli N, Summerfield A, Kida H, Sakoda Y.** N^{pro} of classical swine fever virus contributes to pathogenicity in pigs by preventing type I interferon induction at local replication sites. *Vet Res* 2014;45:1–11.
13. **Szymanski MR, Fiebach AR, Tratschin JD, Gut M, Ramanujam VM, Gottipati K, *et al.*** Zinc binding in pestivirus N^{pro} is required for interferon regulatory factor 3 interaction and degradation. *J Mol Biol* 2009;392:438–449.
14. **Gottipati K, Ruggli N, Gerber M, Tratschin JD, Benning M, Bellamy H, *et al.* Choi KH ebach AR, Guzylack-Piriou L, Python S, Summerfield A, Ruggli N.** The structure of classical swine fever virus N^{pro}: a novel cysteine Autoprotease and zinc-binding protein involved in subversion of type I interferon induction. *PLoS Pathog*

2013;9:e1003704.

15. **Fiebach AR, Guzylack-Piriou L, Python S, Summerfield A, Ruggli N.** Classical swine fever virus N^{pro} limits type I interferon induction in plasmacytoid dendritic cells by interacting with interferon regulatory factor 7. *J Virol* 2011;85:8002–8011.

16. **Kumagai T, Shimizu T, Matumoto M.** Detection of hog cholera virus by its effect on Newcastle disease virus in swine tissue culture. *Science* 1958;28:366.
17. **Fukusho A, Ogawa N, Yamamoto H, Sawada M, Sazawa H.** Reverse plaque formation by hog cholera virus of the GPE^{-} strain inducing heterologous interference. *Infect Immun* 1976;14:332–336.
18. **Mine J, Tamura T, Mitsuhashi K, Okamatsu M, Parchariyanon S, Pinyochon W, *et al.*** The N-terminal domain of N^{pro} of classical swine fever virus determines its stability and regulates type I IFN production. *J Gen Virol* 2015;96:1746–1756.
19. **Sakoda Y, Yamaguchi O, Fukusho A.** A new assay for classical swine fever virus based on cytopathogenicity in porcine kidney cell line FS-L3. *J Virol Methods* 1998;70:93–101.
20. **Sakoda Y, Hikawa M, Tamura T, Fukusho A.** Establishment of a serum-free culture cell line, CPK-NS, which is useful for assays of classical swine fever virus. *J Virol Methods* 1998;75:59–68.
21. **Bensaude E, Turner JL, Wakeley PR, Sweetman DA, Pardieu C, Drew TW, *et al.*** Classical swine fever virus induces proinflammatory cytokines and tissue factor expression and inhibits apoptosis and interferon synthesis during the establishment of long-term infection of porcine vascular endothelial cells. *J Gen Virol* 2004;85:1029–1037.
22. **Agol VI.** Cytopathic effects: Virus-modulated manifestations of innate immunity? *Trends Microbiol* 2012;20:570–576.
23. **Danthi P.** Viruses and the Diversity of Cell Death. *Annu Rev Virol* 2016;3:533–553.
24. **Holler N, Zaru R, Micheau O, Thome M, Attinger A, Valitutti S, *et al.*** Fas triggers an alternative, caspase-8-independent cell death pathway using the kinase RIP as effector molecule. *Nat Immunol* 2000;1:489–495.
25. **Newton K.** RIPK1 and RIPK3: Critical regulators of inflammation and cell death. *Trends Cell Biol* 2015;25:347–353.
26. **Nogusa S, Thapa RJ, Dillon PC, Liedmann S, Oguin HT, Ingram PJ, *et al.*** RIPK3 activates parallel pathways of MLKL-driven necroptosis and FADD-mediated apoptosis to protect against influenza A virus. *Cell Host Microbe* 2017;48:1119–1130.
27. **Wang X, Li Y, Liu S, Yu X, Li L, Shi C, *et al.*** Direct activation of RIP3/MLKL-dependent necrosis by herpes simplex virus 1 (HSV-1) protein ICP6 triggers host antiviral defense. *Proc Natl Acad Sci* 2014;111:15438–15443.

28. **Huang Z, Wu SQ, Liang Y, Zhou X, Chen W, Li L, *et al.*** RIP1/RIP3 binding to HSV-1 ICP6 initiates necroptosis to restrict virus propagation in mice. *Cell Host Microbe* 2015;17:229–242.
29. **Upton JW, Kaiser WJ, Mocarski ES.** Virus inhibition of RIP3-dependent necrosis. *Cell Host Microbe* 2010;7:302–313.
30. **Cho YS, Challa S, Moquin D, Genga R, Ray TD, Guildford M, *et al.*** Phosphorylation-Driven Assembly of the RIP1-RIP3 Complex Regulates Programmed Necrosis and Virus-Induced Inflammation. *Cell* 2009;137:1112–1123.
31. **Berger AK, Hiller BE, Thete D, Snyder AJ, Perez E, Upton JW, *et al.*** Viral RNA at Two Stages of Reovirus Infection Is Required for the Induction of Necroptosis. *J Virol* 2017;91:e02404-16.
32. **Kasza L, Shadduck JA, Christofines GJ.** Establishment, viral susceptibility and biological characteristics of a Swine Kidney cell line SK-6. *Res. vet. Sci.* 1972;13:46–51.
33. **Ruggli N, Tratschin JD, Mittelholzer C, Hofmann MA.** Nucleotide sequence of classical swine fever virus strain Alfort/187 and transcription of infectious RNA from stably cloned full-length cDNA. *J Virol* 1996;70:3478–3487.
34. **Tamura T, Sakoda Y, Yoshino F, Nomura T, Yamamoto N, Sato Y, *et al.*** Selection of Classical Swine Fever Virus with Enhanced Pathogenicity Reveals Synergistic Virulence Determinants in E2 and NS4B. *J Virol* 2012;86:8602–8613.
35. **Mayer D, Thayer TM, Hofmann MA, Tratschin JD.** Establishment and characterisation of two cDNA-derived strains of classical swine fever virus, one highy virulent and one avirulemt. *Virus Res* 2003;98:105–116.
36. **Kameyama K, Sakoda Y, Tamai K, Igarashi H, Tajima M, Mochizuki T, *et al.*** Development of an immunochromatographic test kit for rapid detection of bovine viral diarrhea virus antigen. *J Virol Methods* 2006;138:140–146.
37. **Greiser-Wilke I, Moennig V, Coulibaly COZ, Dahle J, Leder L, Liess B.** Identification of conserved epitopes on a hog cholera virus protein. *Arch Virol* 1990;111:213–225.
38. **Nishimori T, Yamada S, Shimizu M.** Production of Monoclonal Antibodies against Classical Swine Fever Virus and The Use for Antigenic Characterization of Japanese Isolates. *J Vet Med Sci* 1996;58:707–710.
39. **Niwa H, Yamamura KI, Miyazaki JI.** Efficient selection for high-expression transfectants with a novel eukaryotic vector. *Gene* 1991;108:193–200.
40. **Kobasa D, Rodgers ME, Wells K, Kawaoka Y.** Neuraminidase Hemadsorption Activity, Conserved in Avian Influenza A Viruses, Dose Not Influence Viral Replication in Ducks. *J Virol* 1997;71:6706–6713.
41. **Kozasa T, Abe Y, Mitsuhashi K, Tamura T, Aoki H, Ishimaru M, *et al.*** Analysis of

a pair of END^+ and END^- viruses derived from the same bovine viral diarrhea virus stock reveals the amino acid determinants in N^{pro} responsible for inhibition type I interferon production. *J Vet Med Sci* 2015;77:511–518.

42. **Waclawik A, Rivero-Müller A, Rahman NA, Ziecik AJ.** Functional consequences of knocking down porcine prostaglandin synthases in SK-6 swine kidney cell line. *Reprod Biol* 2015;15:42–7.
43. **Sakoda Y, Fukusho A.** Establishment and characterization of a porcine kidney cell line, FS-L3, which forms unique multicellular domes in serum-free culture. *In Vitro Cell Dev Biol Anim* 1998;34: 53–57.
44. **Ruggli N, Tratschin JD, Schweizer M, Mccullough KC, Hofmann MA, Summerfield A.** Classical swine fever virus interferes with cellular antiviral defense: Evidence for a novel function of N^{pro}. *J Virol* 2003;77:7645–7654
45. **Meyers G, Saalmüller A, Büttner M.** Mutations abrogating the RNase activity in glycoprotein E^{rns} of the pestivirus classical swine fever virus lead to virus attenuation. *J Virol* 1999;73:10224–10235.
46. **Aoki H, Sakoda Y, Nakamura S, Suzuki S, Fukusho A.** Cytopathogenicity of classical swine fever viruses that do not show the exaltation of Newcastle disease virus is associated with accumulation of NS3 in serum-free cultured cell lines. *J Vet Med Sci* 2004;66:161–167.
47. **Renson P, Blanchard Y, Dimna ML, Felix H, Cariolet R, Jestin A, *et al.*** Acute induction of cell death-related IFN stimulated genes (ISG) differentiates highly from moderately virulent CSFV strains. *Vet Res* 2010;41:7.
48. **Choi C, Hwang KK, Chae C.** Classical swine fever virus induces tumor necrosis factor-α and lymphocyte apoptosis. *Arch Virol* 2004;149:875–889.
49. **Summerfield A, McNeilly F, Walker I, Allan G, Knoetig SM, McCullough KC.** Depletion of CD4+ and CD8high+ T-cells before the onset of viraemia during classical swine fever. *Vet Immunol Immunopathol* 2001;78:3–19.
50. **Fan S, Yuan J, Deng S, Chen Y, Xie B, Wu K, *et al.*** Activation of Interleukin-1β Release by the Classical Swine Fever Virus Is Dependent on the NLRP3 Inflammasome, Which Affects Virus Growth in Monocytes. *Front Cell Infect Microbiol* 2018;8:1–13.
51. **Gou H, Zhao M, Xu H, Yuan J, He W, Zhu M, *et al.*** CSFV induced mitochondrial fission and mitophagy to inhibit apoptosis. *Oncotarget* 2017;8:39382–39400.
52. **Pei J, Deng J, Ye Z, Wang J, Gou H, Liu W, *et al.*** Absence of autophagy promotes apoptosis by modulating the ROS-dependent RLR signaling pathway in classical swine fever virus-infected cells. *Autophagy* 2016;12:1738–1758.
53. **Kümmerer BM, Tautz N, Becher P, Thiel HJ, Meyers G.** The genetic basis for cytopathogenicity of pestiviruses. *Vet Microbiol* 2000;77:117–128.
54. **Meyers G, Thiel HJ.** Cytopathogenicity of classical swine fever virus caused by

defective interfering particles. *J Virol* 1995;69:3683–3689.

FIGURE LEGENDS

Fig. 1. Morphological changes and cell viability of CPK-NS and CPK cells infected with different CSFV clones. (A) Schematic representation of genomes of vGPE^{-} and vALD-A76 clones. The amino acids differences are shown at positions 5, 27, 32 (gray) and 136 (black) in the N^{pro}. The position 136 is responsible for inhibition of type-I interferon (IFN) production in vALD-A76. The white and grey boxes indicate the nonstructural proteins and the structural proteins, respectively. (B) Cytopathic effect (CPE) of the cells were observed every 24 h after inoculation of the CSFV clones indicated above each panel or treatment with recombinant swine interferon alpha (swIFN-α) or cisplatin. The images were captured at 96 h after inoculation of the CSFV clones of treatment with swIFN-α or cisplatin. The scale bar indicates 100 μm. (C) Cell viability was assessed at the indicated time points after infection with the CSFV clones or treatment with swIFN-α or cisplatin. The OD_{450} values in mock-infected cells at each time point were considered as 100% viability. The results are indicated as the mean values of three independent experiments with error bars representing the standard error of the mean. *: $p<0.01$ compared to the cells infected with vALD-A76. (D, E) The inhibition of CPE at 96 hr post infection or cell death by using antiserum against swIFN-α (anti-IFN) was monitored. CPK-NS cells were treated with swIFN-α or inoculated with vGPE^{-} immediately followed by the addition of anti-IFN in the medium. The scale bar indicates 100 μm. (E) The OD_{450} values in mock-infected or mock-treated cells without antiserum treatment at each time

point were considered as 100% viability. The results are indicated as the mean values of four independent experiments with error bars representing the standard error of the mean. * $p<0.01$, cell viability of swIFN-α + anti-IFN-treated cells compared to swIFN-α-treated cells. # $p<0.01$, indicates cell viability of $vGPE^-$ + anti-IFN-treated cells compared to $vGPE^-$-infected cells.

Fig. 2. Cell viability of CPK-NS cells infected with $vGPE^-$ or treated with swIFN-α or cisplatin in the presence of cell-death inhibitors. CPK-NS cells were inoculated with $vGPE^-$ or treated with swIFN-α or cisplatin. Caspase-3 inhibitor, caspase-8 inhibitor, and receptor interacting protein kinase-1 (RIPK1) inhibitor were added immediately after virus inoculation or IFN or cisplatin treatment. Cell viability was assessed at 96 hpi. The OD_{450} value in mock-infected or mock-treated cells with each inhibitor was set to 100% viability. The results are indicated as the mean values of three independent experiments with error bars representing the standard error of the mean. *: $p<0.01$.

Fig. 3. The expression levels of cell-death related proteins in CPK-NS and CPK cells. Cells were inoculated with CSFV clones or treated with swIFN-α or cisplatin. (A) Cell lysates of CPK-NS cells (left) and CPK cells (right) were obtained at the indicated time points and assessed by using Western blotting and immunodetection with antibodies against Caspase-3, PARP, MLKL, phosphorylated MLKL, and GAPDH (serving as a loading control). (B) Relative expression of

MLKL and phosphorylated-MLKL in CPK-NS cells at 72 and 96 hpi. Expression signals were quantified by using ImageJ and described as the relative expression level of target protein/GAPDH ratio. The ratio for mock-infected cells were set to a value of 1. The results are indicated as the mean values of three independent experiments with error bars representing the standard error of the mean. * $p<0.01$, compared to mock-infected cells.

Fig. 4. Apoptosis activation in CPK-NS cells infected with different CSFVs. CPK-NS cells were inoculated with CSFV clones at MOI=1.0 $TCID_{50}$/cell (A) or at the indicated MOI (B, C). (A, B) Caspase-3/7 activity was assessed by Caspase-3/7 Glo assay at the indicated time points. Caspase-3/7 activity is represented as relative luminescence measurement compared with mock-infected cells. The results are indicated as the mean values of three independent experiments with error bars representing the standard error of the mean. *: $p<0.01$ compared to cells at 0 hpi. (C) Cell viability was assessed at the indicated time points. The OD_{450} value in mock-infected cells was set to 100% viability. The results are indicated as the mean values of three independent experiments with error bars representing the standard error of the mean. *: $p<0.01$ compared to cells at 0 hpi.

Fig. 5. Caspase-3/7 activity and cell viability of CPK-NS cells infected with vALD-A76/N362S.

(A) Schematic representation of the vGPE^{-} and vALD-A76 genomes. A single amino-acid difference was found in E^{rns} between these two clones. The white, grey, and dark grey boxes indicate the nonstructural proteins, the structural proteins, and the RNase domains (amino acids 295-307 and 338-357), respectively. (B) CPK-NS cells were inoculated with CSFV clones at MOI=1.0 $TCID_{50}$/cell. Caspase-3/7 activity was assessed by using Caspase-3/7 Glo assay at the indicated time points. Caspase-3/7 activity is presented as relative luminescence measurement in comparison with mock-infected cells. The results are indicated as the mean values of three independent experiments with error bars representing the standard error of the mean. *: $p<0.01$ compared to cells infected with vALD-A76 at each time point. (C) Cell viability was assessed at the indicated time points after infection with MOI=1.0 $TCID_{50}$/cell of CSFV clones. The OD_{450} values in mock-infected cells at each time point were considered as 100% viability. The results are indicated as the mean values of three independent experiments with error bars representing the standard error of the mean. (D) Semi-confluent monolayers of SK-6 cells were infected in 6-well plates (10 cm^2 wells) with vALD-A76, vALD-A76/N362S, vEy/H297K or mock or left untreated. After 24 h of incubation with complete medium, the cells were washed 5 times with PBS and cultured for another 16 h in serum-free EMEM. Cell extracts were obtained by hypotonic lysis with H_2O (400 µl per well). The Dy-781-O1-RNA probe was then incubated with EMEM containing RNase A or with the cell extracts at the indicated dilutions and finally separated by urea/polyacrylamide gel electrophoresis. The star indicates the position

of undigested RNA probe. (E) Proteins from cells from replica wells infected as in (D) were extracted as indicated in materials and methods and separated by SDS-PAGE. The proteins were then transferred to Immun-blot LF PVDF membranes. E2 and β-actin were detected with HC/TC26 and anti-β-actin antibodies and with IRDye680-labeled as secondary antibody.

Fig. 6. Expression of CSFV proteins in CPK-NS cells. CPK-NS cells were inoculated with CSFV clones at MOI=1.0 $TCID_{50}$/cell. Cell lysates were obtained at the indicated time points. (A) CSFV NS3 and NS2-3 were detected using Western blotting. (B) Expression signals were quantified by CS Analyzer 4 and described as the NS3/NS2-3 ratio. (C) CSFV E2 was detected using dot blotting. (D) Expression signals of E2 were quantified by using a CS Analyzer 4 and described as relative expression of CSFV-infected cells *versus* mock-infected cells. (E) CPK-NS cells were inoculated with vALD-A76 at MOI=1.0 $TCID_{50}$/cell and treated with 2×10^5 unit/cell of swIFN-α or 50 μM of cisplatin. Cell lysates were obtained at the indicated time points. CSFV NS3 and NS2-3 were detected by Western blotting. (F) Expression signals were quantified by CS Analyzer 4 and described as the NS3/NS2-3 ratio.

Fig. 7. Model of the molecular mechanisms of the cell-death signaling pathways regulated in CPK-NS cells infected with CSFV. (A) In the case of a cloned virulent strain vALD-A76, viral

protein N^{pro} degrades IRF-3 to suppress type-I interferon production and subsequent necroptosis. (B) In the case of the cloned vaccine strain vGPE^{-}, N^{pro} is unfunctional in inhibition of IFN induction. vGPE^{-} cannot inhibit necroptosis nor apoptosis triggered by type-I IFN or double-stranded RNA. Type-I IFN production is required for evident CPE in CPK-NS cells. Other viral factor(s) than E^{rns} may be involved in apoptosis inhibition by vALD-A76 and apoptosis induction by vGPE^{-} in CPK-NS cells (A and B).

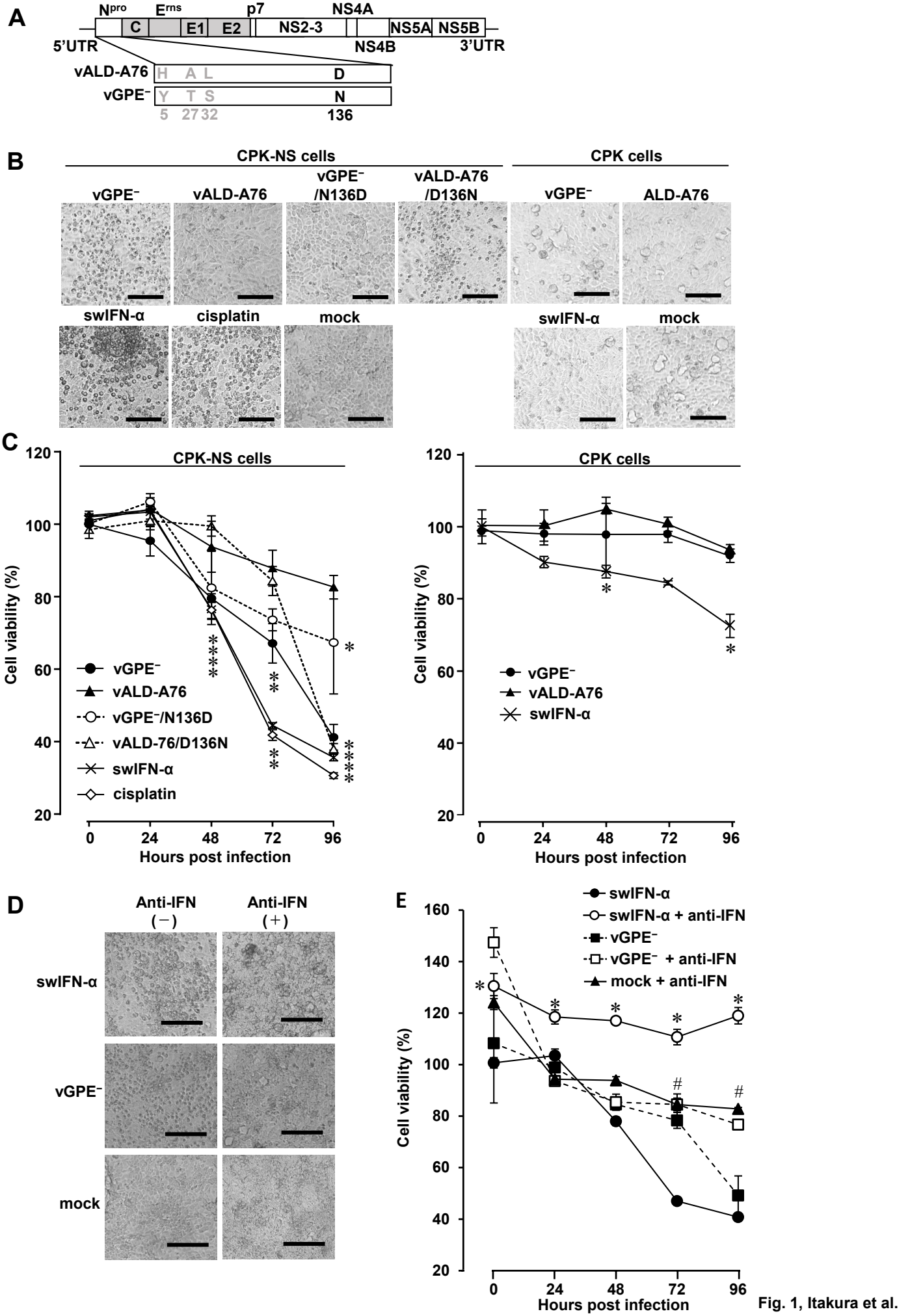

Fig. 1, Itakura et al.

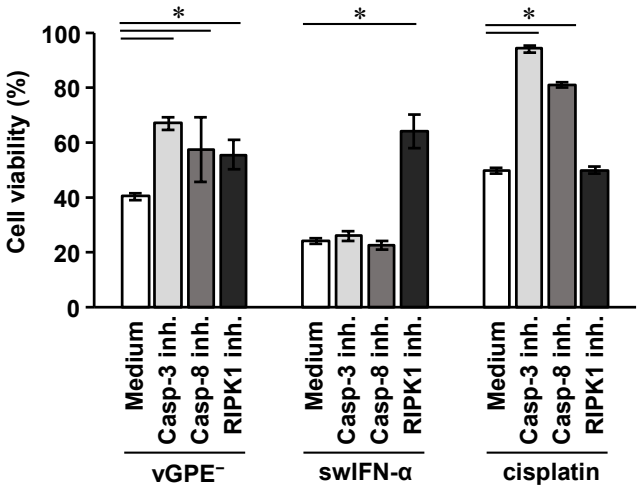

Fig. 2, Itakura et al.

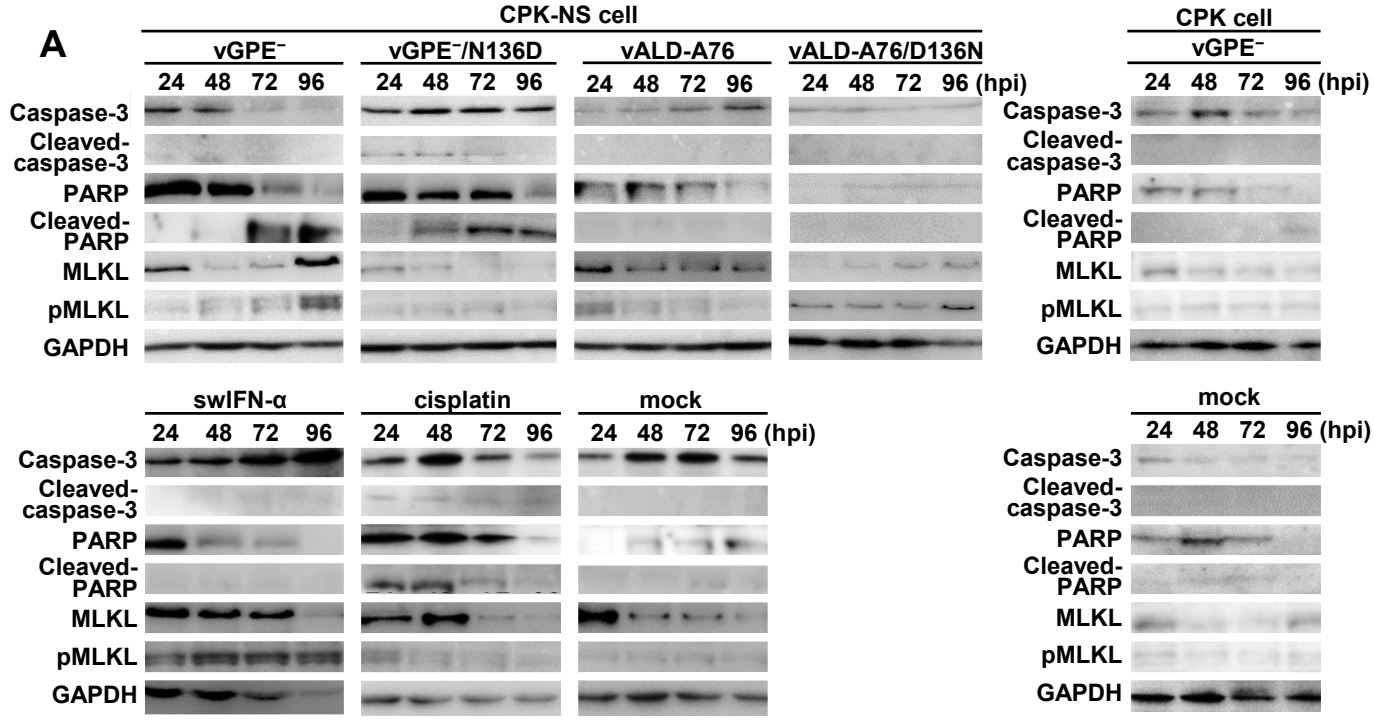

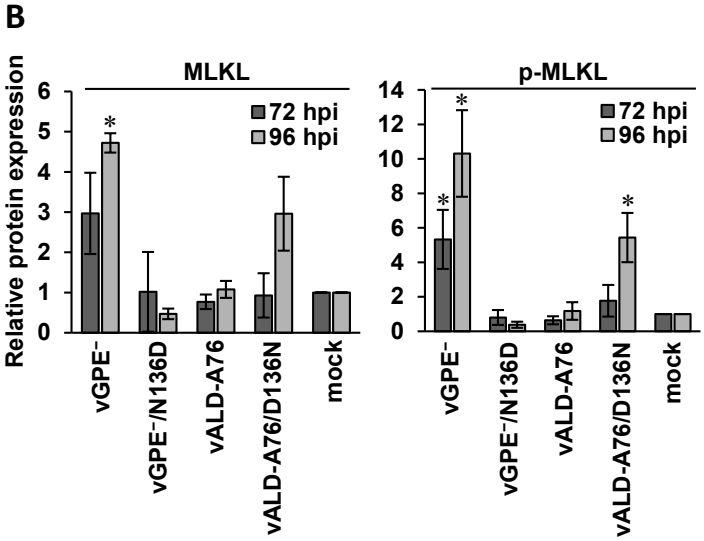

Fig. 3, Itakura et al.

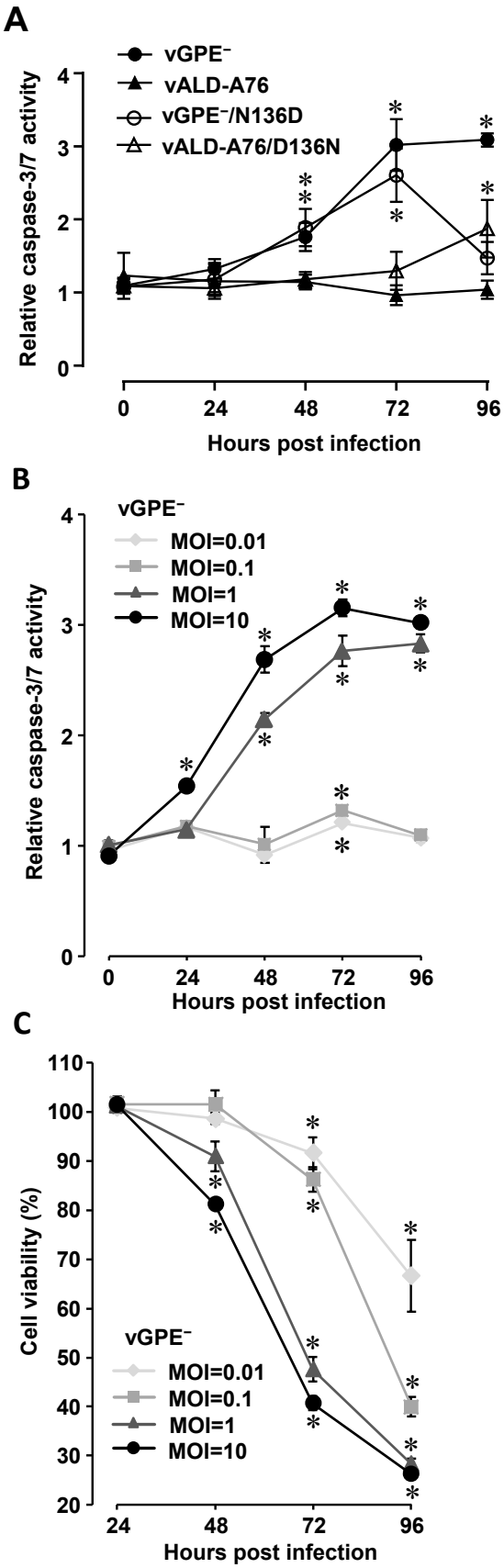

Fig. 4, Itakura et al.

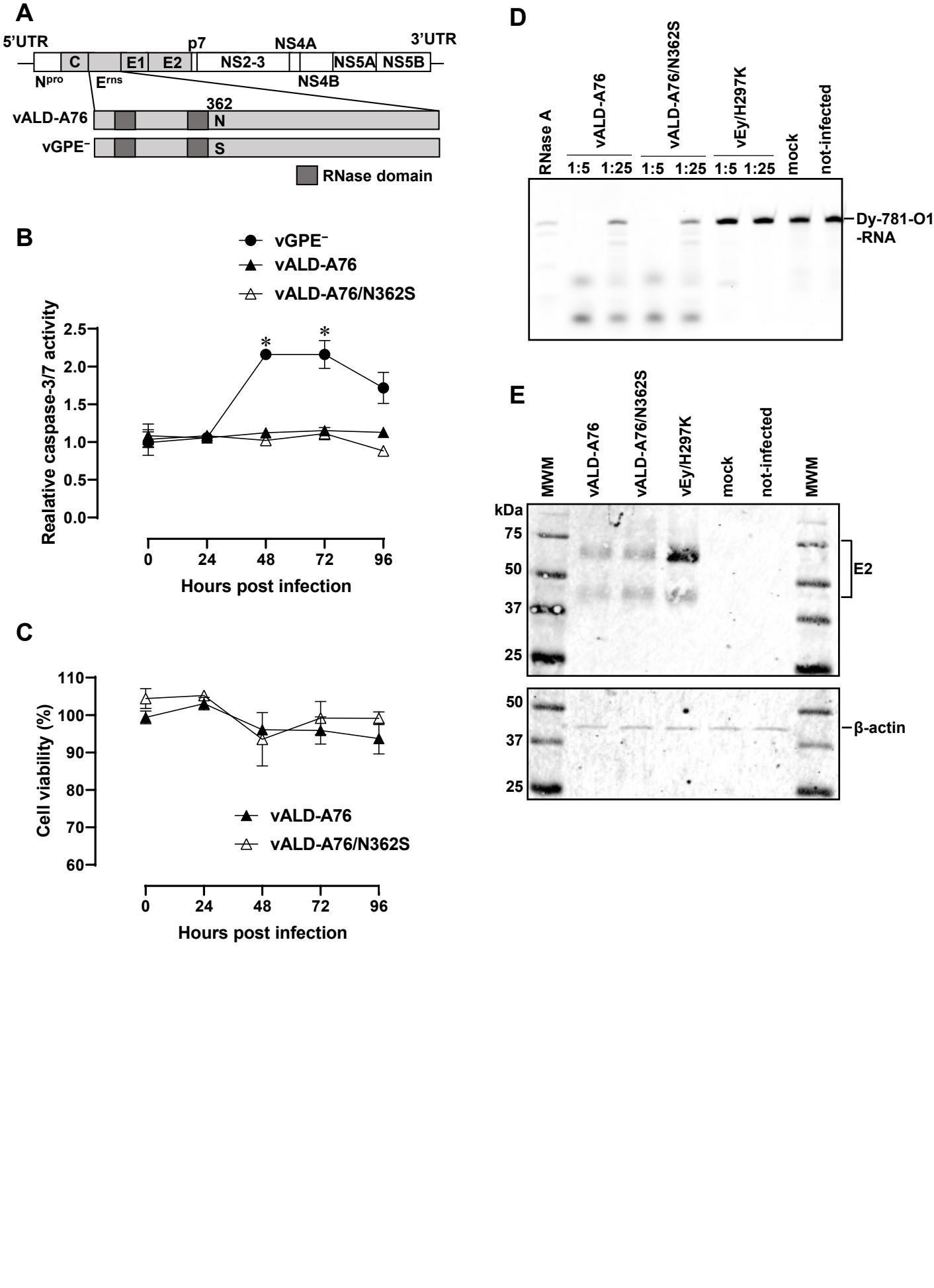

Fig. 5, Itakura et al.

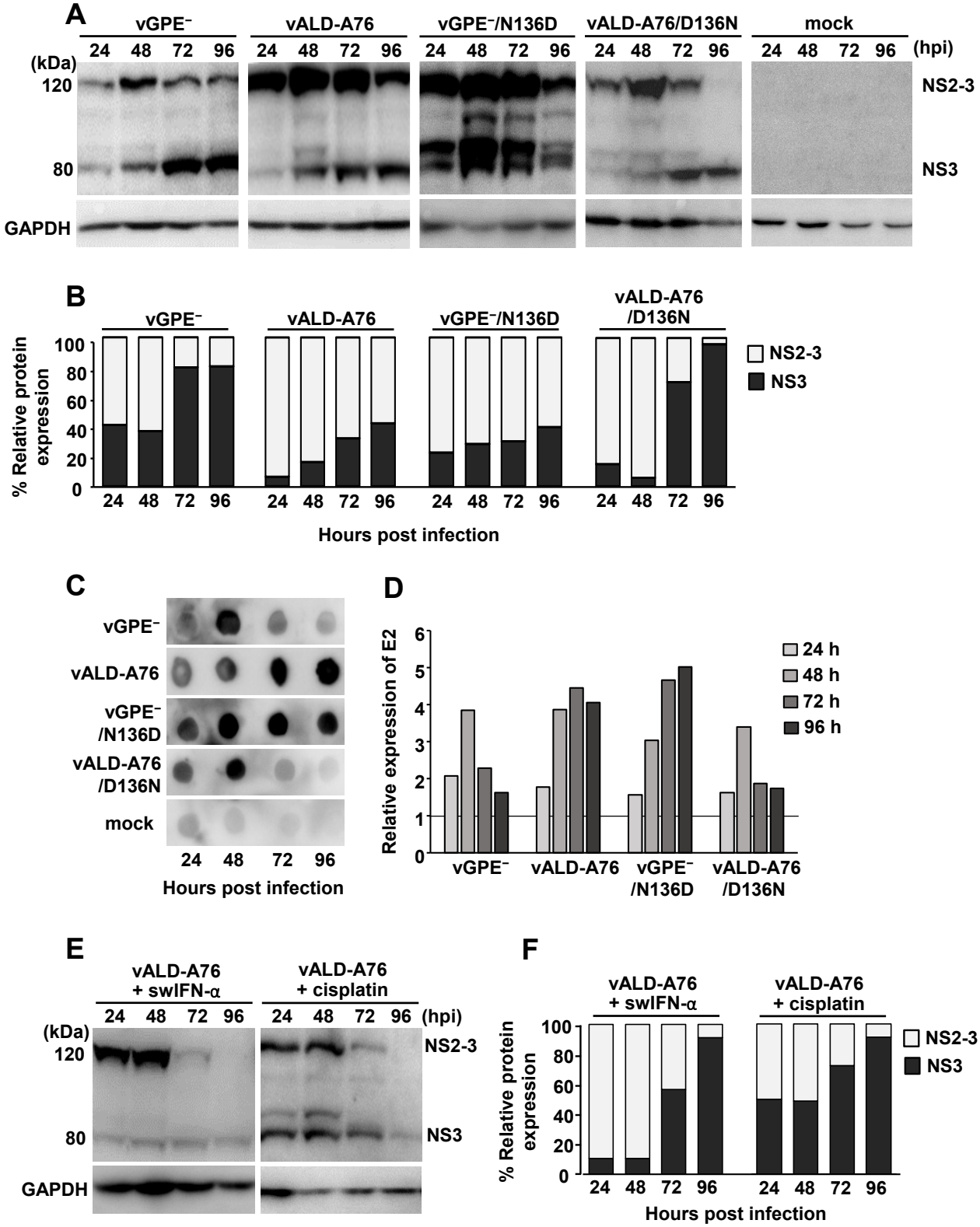

Fig. 6, Itakura et al.

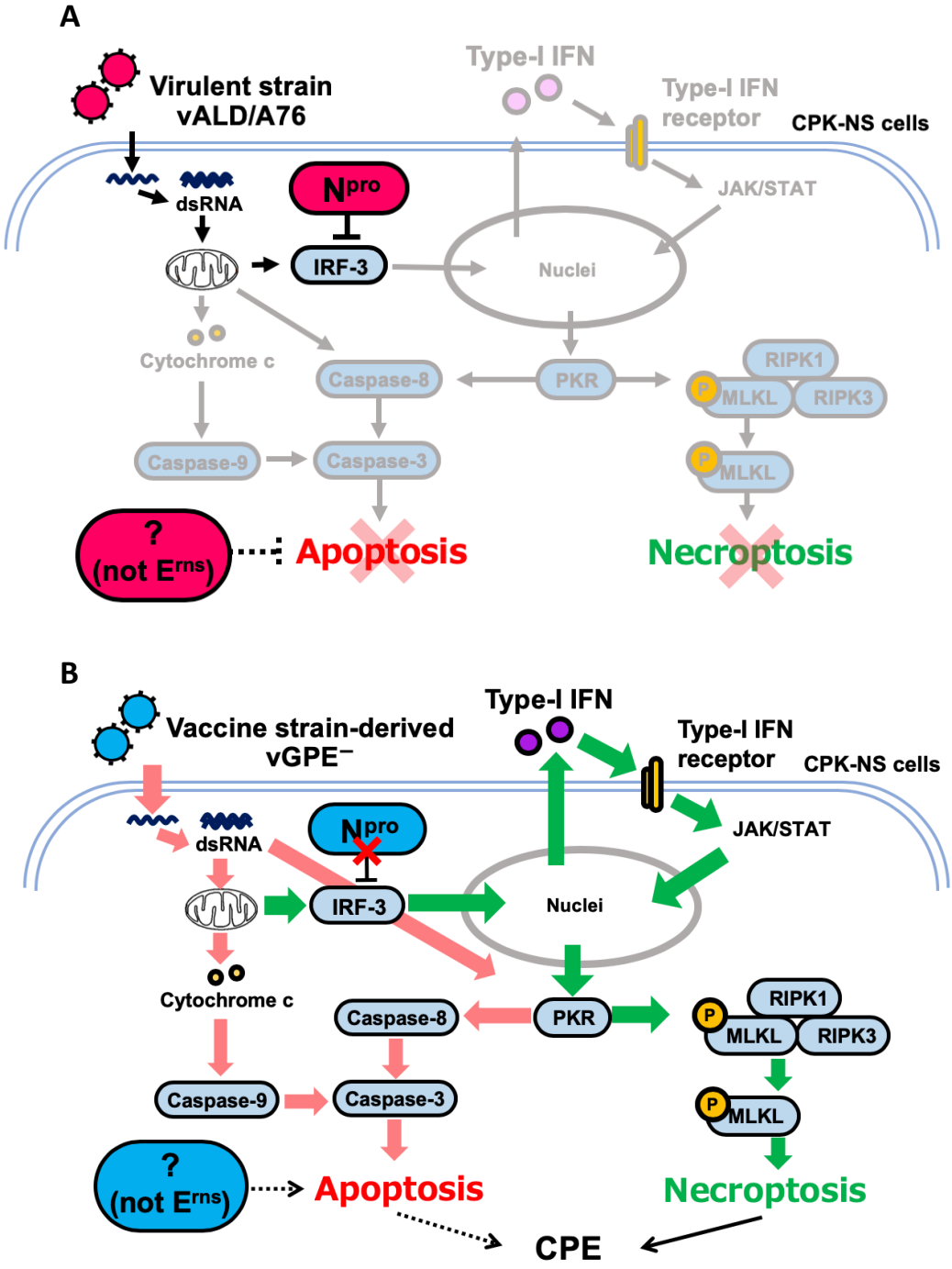

Fig. 7, Itakura et al.